

Electrochromic Platinum(II) Complexes Derived from Azobenzene and Zwitterionic Quinonoid Ligands: Electronic and Geometric Structures

Naina Deibel,[†] Stephan Hohloch,[‡] Michael G. Sommer,[‡] David Schweinfurth,[‡] Fabian Ehret,[†] Pierre Braunstein,[§] and Biprajit Sarkar^{*‡}

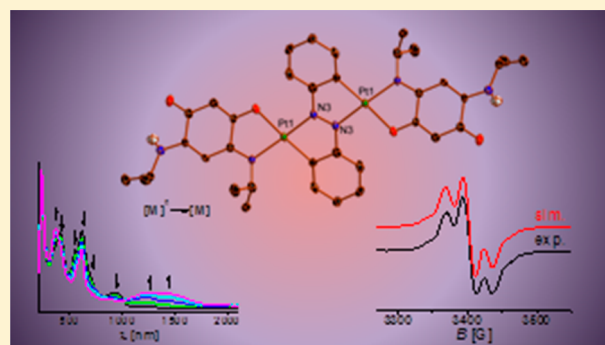
[†]Institut für Anorganische Chemie, Universität Stuttgart, Pfaffenwaldring 55, D-70569 Stuttgart, Germany

[‡]Institut für Chemie und Biochemie, Freie Universität Berlin, Fabeckstraße 34-36, D-14195 Berlin, Germany

[§]Laboratoire de Chimie de Coordination, Institut de Chimie (UMR 7177 CNRS), Université de Strasbourg, 4 rue Blaise Pascal, 67081 Strasbourg Cedex, France

Supporting Information

ABSTRACT: The ligands azobenzene (az) and the zwitterionic 4-(isopropylamino)-6-(isopropyliminio)-3-oxocyclohexa-1,4-dien-1-olate (Q) were used to synthesize the mononuclear complex $[(Q_H)Pt(az_H)]$ (1), and the dinuclear complex $[(Q_H)Pt(\mu\text{-}az_{2H})Pt(Q_H)]$ (2). Structural characterization of the complexes shows a distorted-square-planar environment around the Pt(II) centers and localization of the double bonds within the Q_H ligand on metal coordination. Furthermore, the N=N azo bond is elongated in the metal complexes in comparison to free az, owing to π back-bonding from Pt(II) to az. Complexes 1 and 2 display multiple reversible reduction steps in their cyclic voltammograms. The complexes also exhibit strong absorptions in the visible region, the position and intensity of which can be influenced by the chromophore $[(Q_H)Pt]$. UV-vis-near-IR spectroelectrochemical studies show that the absorption of these complexes in the visible as well as the near-IR region can be controlled by electron transfer steps. Depending on the charge state of the complexes, they are found to be either transparent in the near-IR region but strongly absorbing in the visible or vice versa, thus displaying strong electrochromic behavior. EPR spectroelectrochemical studies together with DFT calculations and comparison with the complex $[(Q_H)Pd(az_H)]$ (3) are used to locate the site of electron transfer in these complexes and to elucidate their electronic properties in the various redox states. Complex 2 is a rare example where doubly deprotonated azobenzene acts as a bridging ligand.



INTRODUCTION

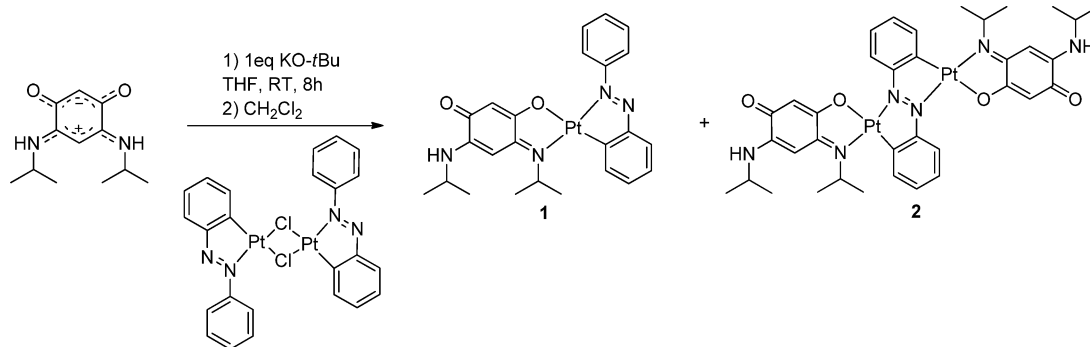
The compound azobenzene (az) has been extensively used for “molecular switching” purposes because of its ability to undergo reversible light-induced isomerism.¹ Intriguingly, az was also one of the first ligands where C–H activation was observed in its Pd(II) and Pt(II) complexes.² Azo ligands in general have been widely used in coordination and organometallic chemistry because of their redox non-innocent character and their ability to strongly absorb light in the visible or the near-IR region in their metal-coordinated forms.³ Metal complexes of azo ligands such as phenylazopyridine and 2,2'-azobispyridine⁴ have been extensively studied, and those with az_H as a chelating ligand have also been investigated.^{1c–e,5} However, the use of az_{2H} as a bis-chelating bridging ligand toward metal centers has been only sporadically reported.⁶

The zwitterionic molecule 4-(isopropylamino)-6-(isopropyliminio)-3-oxocyclohexa-1,4-dien-1-olate (Q) and other members of the series with different N substituents have been shown previously to possess many fascinating properties.⁷ Recently,

properties of these and related ligands on various surfaces have been explored.⁸ Metal complexes of these ligands in their deprotonated forms have displayed unusual bonding and electronic properties.^{7,9} Such complexes have found use in homogeneous catalysis,¹⁰ supramolecular chemistry,^{7c} and electron transfer research.¹¹ The “para” counterparts of these ligands have also been explored by us¹² and others¹³ in recent years in various areas of coordination and organometallic chemistry. Our continuing interest in the redox and electronic properties of metal complexes containing quinonoid and azo type ligands, and the knowledge of the excellent light absorption properties of az, Q, and their deprotonated forms led us to the present project. Here we have combined these two classes of ligands on the platform of a d^8 Pt(II) center which is predestined to form square-planar complexes. We present below the mononuclear complex $[(Q_H)Pt(az_H)]$ (1) and the

Received: September 13, 2013

Scheme 1. Synthesis of Complexes 1 and 2



dinuclear complex $[(Q_{-H})Pt(\mu\text{-az}_{-2H})Pt(Q_{-H})]$ (**2**), with the monodeprotonated form of **Q** and the mono- and dideprotonated forms of **az**. A combination of structural, electrochemical, and UV–vis–near-IR and EPR spectroelectrochemical studies and support from DFT calculations are used to shed light on the electronic structures of these complexes in their various accessible redox forms. We explore below the possibility of switching the absorption properties of these complexes in the visible and the near-IR region through redox processes. Insights from the combined studies are used to understand this electrochromic behavior and to locate the sites of electron transfers in these molecules. The known complex $[(Q_{-H})Pd(\text{az}_{-H})]$ (**3**)^{11f} will be used for comparison purposes and for a better understanding of the complexes presented in this study.

RESULTS AND DISCUSSION

Synthesis and Crystal Structures. The mono- and dinuclear complexes **1** and **2** were both synthesized by the reaction of Q^{11d} with $[(\text{az}_{-H})Pt(\mu\text{-Cl})_2Pt(\text{az}_{-H})]^2$ in the presence of a base (Scheme 1). Extraction with *n*-heptane led to the separation of red **1** from blue **2**, and subsequent recrystallization led to the isolation of pure products for both complexes (see the Experimental Section).

The identity and purity of the products were established by ¹H and ¹³C NMR spectroscopy, elemental analysis, and mass spectrometry. The N–H proton of Q_{-H} , which appears at 6.58 and 6.64 ppm for **1** and **2**, respectively, appears as a doublet (Figure S1, Supporting Information). The appearance of the doublet is a result of the coupling of the N–H proton with the C–H proton of the isopropyl substituent on the nitrogen atom of Q_{-H} . While identical reaction conditions were used to synthesize the Pd(II) analogues, only the mononuclear complex **3** could be isolated, as reported previously.^{11f} Increasing the amount of base, the reaction time, or the temperature did not lead to the formation of a dinuclear complex in the case of Pd(II). Thus, Pt(II) is seen to favor the double deprotonation of **az**, which then acts as a bridging ligand in **2**. It should be noted here that although **az** in its monodeprotonated, ortho-metalated form has been extensively used as a chelating ligand in many metal complexes since the pioneering work by Cope and Siekman,² its use as a bridging ligand in its doubly deprotonated form has been rare.⁶ Attempts at deprotonating the remaining N–H protons of **2**, with the aim of generating multinuclear complexes, were unfortunately not successful. Such reactions led to the formation of **1** and other unidentified decomposition products.

Single crystals of **1**·0.5CH₂Cl₂ suitable for X-ray diffraction studies were grown by layering a dichloromethane solution with

n-hexane followed by slow diffusion at ambient temperature. The same was achieved for **2**·0.5C₃H₆O by slow diffusion of diethyl ether into an acetone solution (see the Experimental Section). **1**·0.5CH₂Cl₂ crystallizes in the monoclinic *C2/c* space group and **2**·0.5C₃H₆O in the orthorhombic *Pbcn* space group (Table S1, Supporting Information). The Pt(II) center in **1**·0.5CH₂Cl₂ is in a distorted-square-planar environment, being coordinated by the C and N centers of the az_{-H} ligand and the O and N centers of the Q_{-H} ligand (Figure 1). The distortion is imposed by the chelating nature of both ligands (Table 1).

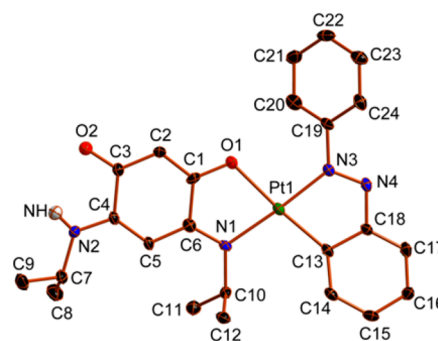


Figure 1. ORTEP view of **1**·0.5CH₂Cl₂. Ellipsoids are drawn at 50% probability. The hydrogen atoms and solvent molecules have been omitted for clarity.

Table 1. Selected Bond Angles (in deg) in the Complexes

	1 ·0.5CH ₂ Cl ₂	2 ·0.5C ₃ H ₆ O	3 ^a
O1–Pt1–N1/O1–Pd1–N1	78.81(8)	78.4(2)	78.8(1)
N1–Pt1–C13/N1–Pd1–C13	105.14(9)	103.6(3)	107.7(1)
C13–Pt1–N3/C13–Pd1–N3	78.28(9)	78.7(3)	78.5(1)
N3–Pt1–O1/N3–Pd1–O1	98.07(7)	101.7(2)	95.2(1)
N3–Pt1–N1/N3–Pd1–N1	175.15(8)	168.3(3)	172.1(1)
C13–Pt1–O1/C13–Pd1–O1	173.98(8)	168.4(3)	173.5(1)

^aFrom ref 11f.

In **2**·0.5C₃H₆O, both Pt(II) centers are in a distorted-square-planar environment, each of them being coordinated by the C and N atoms of the az_{-2H} ligand and the O and N donors of the Q_{-H} ligands (Figure 2). The az_{-2H} ligand thus acts as a bridge between the two Pt(II) centers in **2**·0.5C₃H₆O. The molecule possesses an inversion center at the N=N azo bond.

The Pt–O, Pt–N, and Pt–C bond lengths in both complexes are in the expected range (Table 2). The Pt1–N3 distance to the azo-N is slightly shorter than the Pt1–N1 distance to the Q_{-H} ligand. As reported previously, in the free

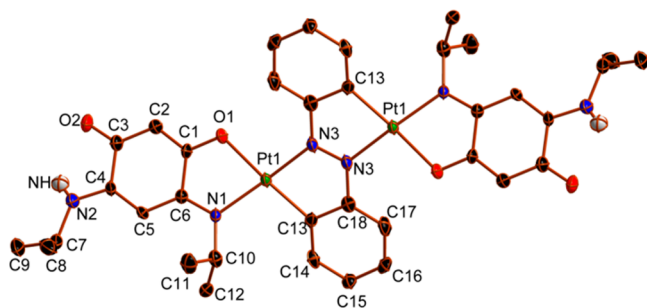


Figure 2. ORTEP plot of $2 \cdot 0.5C_3H_6O$. Ellipsoids are drawn at 50% probability. The hydrogen atoms and solvent molecules have been omitted for clarity.

Table 2. Selected Bond Lengths in the Complexes (in Å)

	$1 \cdot 0.5CH_2Cl_2$	$2 \cdot 0.5C_3H_6O$	3^a
Pt1–O1/Pd1–O1	2.082(2)	2.092(5)	2.058(2)
Pt1–C13/Pd1–C13	1.995(2)	1.973(7)	1.995(3)
Pt1–N3/Pd1–N3	1.993(2)	2.015(6)	2.018(3)
Pt1–N1/Pd1–N1	2.024(2)	2.035(6)	2.078(3)
C1–O1	1.317(3)	1.298(9)	1.286(4)
C3–O2	1.241(3)	1.23(1)	1.236(4)
C1–C2	1.364(3)	1.37(1)	1.363(5)
C2–C3	1.420(4)	1.41(1)	1.404(5)
C3–C4	1.524(4)	1.52(1)	1.519(5)
C4–C5	1.373(3)	1.37(1)	1.371(5)
C5–C6	1.404(3)	1.40(1)	1.411(5)
C6–C1	1.480(4)	1.50(1)	1.509(5)
C6–N1	1.331(3)	1.330(9)	1.317(5)
C4–N2	1.328(3)	1.33(1)	1.331(5)
N3–N4/N3–N3	1.278(3)	1.30(1)	1.269(4)
N3–C19/N3–C18	1.446(3)	1.42(1)	1.437(4)
N4–C18/N3–C18	1.394(3)	1.42(1)	1.398(5)

^aFrom ref 11f.

ligand Q_L electronic delocalization is observed in the “upper” and “lower” parts of the molecule, which are connected to each other with two C–C single bonds.⁷ Such a situation results in a $6\pi + 6\pi$ system for ligands such as Q_L . For $1 \cdot 0.5CH_2Cl_2$, the C1–O1 bond distance within Q_{H1} is 1.317(3) Å and the C3–O2 distance is 1.241(3) Å. Accordingly, the C1–C2 distance is 1.364(3) Å and the C2–C3 distance is 1.420(4) Å. A similar trend is observed in the “lower” part of Q_{H1} in $1 \cdot 0.5CH_2Cl_2$: the

C4–C5 bond distance of 1.373(3) Å is shorter than the C5–C6 distance of 1.404(3) Å; the C–N bond distances, however, are more similar. Thus, monodeprotonation and coordination to a single metal center leads to bond localization within Q_{H1} . The C3–C4 and C6–C1 distances of about 1.5 Å are in the range of a single bond, just as in the case of free Q_L (Table 2). The bonding situation within the Q_{H1} ligand in $2 \cdot 0.5C_3H_6O$ is exactly the same as in $1 \cdot 0.5CH_2Cl_2$. Similar to the case for $1 \cdot 0.5CH_2Cl_2$, in $2 \cdot 0.5C_3H_6O$, Q_{H1} is bound to a single metal center, and hence bond localization is observed within that ligand in $2 \cdot 0.5C_3H_6O$ (Table 2). Similar trends have been observed for Q_{H1} in 3^{11f} and in other related complexes where Q_{H1} is coordinated to a single metal center.¹¹ The N=N bond length in az_{H1} in $1 \cdot 0.5CH_2Cl_2$ is 1.278(3) Å. The corresponding value within az_{2H1} in $2 \cdot 0.5C_3H_6O$ is 1.30(1) Å. Coordination of metal centers to az_{H1} or az_{2H1} leads to back-bonding from the filled $d\pi$ orbitals of Pt(II) to the empty π^* orbitals of the azo ligand, leading to an elongation of the N=N bond in comparison to free azobenzene.^{3,4,5b} The intramolecular Pt–Pt distance in $2 \cdot 0.5C_3H_6O$ is 4.78 Å.

The presence of uncoordinated “O” and “N–H” sites within Q_{H1} in both $1 \cdot 0.5CH_2Cl_2$ and $2 \cdot 0.5C_3H_6O$ leads to intermolecular hydrogen bonding in these molecules in the solid state. In the mononuclear complex $1 \cdot 0.5CH_2Cl_2$, hydrogen bonding between complementary N–H and O groups of two adjacent molecules leads to the formation of dimers in the solid state (Figure 3). The N–H...O distance is 2.30(2) Å. For the dinuclear complex $2 \cdot 0.5C_3H_6O$, the presence of two Q_{H1} ligands within the complex allows hydrogen bonding in both directions. Such weak intermolecular interactions lead to the formation of a three-dimensional “steplike” structure in the solid state (Figure 3). The N–H...O distance between two molecules of $2 \cdot 0.5C_3H_6O$ is 2.5(1) Å.

Cyclic Voltammetry. The redox properties of complexes **1** and **2** were investigated by cyclic voltammetry. **1** displays two reversible reduction steps at -1.58 and -1.93 V in $CH_2Cl_2/0.1$ M Bu_4NPF_6 (Figure 4 and Table 3). The difference between these reduction potentials is 350 mV. For comparison, the corresponding mononuclear Pd(II) complex **3** shows two reduction steps at -1.56 and -1.85 V, respectively, with a potential difference of 290 mV.^{11f} Hence, the replacement of Pd(II) by Pt(II) on going from **3** to **1** appears to increase the thermodynamic stability of the one-electron-reduced form; the comproportionation constant K_C values are on the order of 10^5

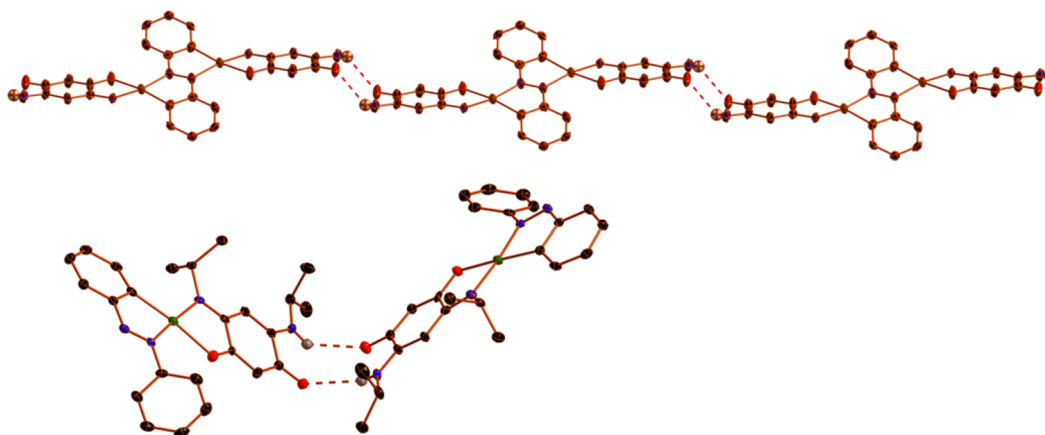


Figure 3. Intermolecular hydrogen bonding in $1 \cdot 0.5CH_2Cl_2$ (top) and $2 \cdot 0.5C_3H_6O$ (bottom).

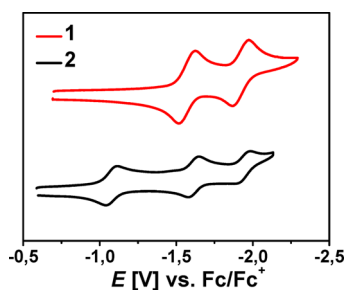


Figure 4. Cyclic voltammograms of **1** and **2** in $\text{CH}_2\text{Cl}_2/0.1 \text{ M Bu}_4\text{NPF}_6$ at 295 K. Scan rate: 100 mV/s. The ferrocene/ferrocenium couple was used as an internal standard.

Table 3. Redox Potentials of Complexes from Cyclic Voltammetry^a

compd	$E^{\text{ox}1}$ (V)	$E^{\text{red}1}$ (V) ^d	$E^{\text{red}2}$ (V) ^d	$E^{\text{red}3}$ (V) ^d
1		-1.58 (90)	-1.93 (95)	
2		-1.08 (65)	-1.62 (65)	-1.94 (70)
3^b	0.80 ^c	-1.56	-1.85	

^aHalf-wave potentials from cyclic voltammetric measurements in $\text{CH}_2\text{Cl}_2/0.1 \text{ M Bu}_4\text{NPF}_6$ for reversible processes at 298 K and a scan rate of 100 mV s⁻¹, with ferrocene/ferrocenium used as an internal standard. ^bFrom ref 11f. ^c E_{pa} for the irreversible process. ^dPeak to peak separations in mV are given in parentheses.

and 10^6 for $3^{\bullet-}$ and $1^{\bullet-}$, respectively. The uncoordinated ligand Q is known to display only irreversible reduction processes.

Complex **2**, which contains two “Pt(Q_H)” units and a doubly deprotonated az_{2H} bridging ligand, displays three reversible reduction steps, the first of which appears at -1.08 V (Figure 4). Thus, going from the mononuclear Pt(II) complex **1** to the dinuclear Pt(II) complex **2** results in an anodic shift of 500 mV for the first reduction step (Table 3). Furthermore, the removal of a proton from az_H and the addition of the second “Pt(Q-H)” unit on going from **1** to **2** also results in the appearance of an additional, third reduction step. Metal coordination is known to result in a positive shift of the reduction potentials of azo ligands.^{3,4} The difference between the first and second reduction processes of **2** is 540 mV, and this translates to a K_{c} value on the order of 10^9 for the one-electron-reduced form of **2**, a value that is substantially higher than that of the one-electron-reduced form of the corresponding mononuclear complex **1**. For the mononuclear Pd(II) complex **3**, an irreversible oxidation process was observed at 0.80 V.^{11f} For **1** and **2**, no oxidation step was detected within the dichloromethane solvent window. In order to further shed light on the electronic structures of the various redox forms, and to possibly locate the site of electron transfer in **1** and **2**, spectroscopic signatures were collected for the various redox forms of the complexes, and DFT calculations were carried out.

EPR Spectroscopy and Spin-Density Calculations. The one-electron- and two-electron-reduced forms of the complexes were generated either chemically or electrochemically (see the Experimental Section), and the X-band EPR spectra of those species were recorded. The one-electron-reduced form of the mononuclear Pt(II) complex $1^{\bullet-}$ in CH_2Cl_2 displays an isotropic signal at 295 K centered at $g = 1.986$ (Figure 5). No hyperfine structure was detected for this species. The g -value and the appearance of the EPR signal in fluid solution at 295 K are the first signs of a ligand-centered spin.¹⁴ The corresponding mononuclear Pd(II) complex $3^{\bullet-}$ displays an

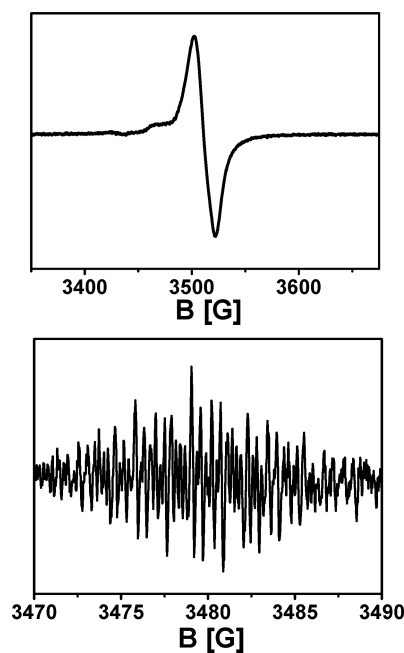


Figure 5. X-band EPR spectra of chemically generated $1^{\bullet-}$ (top) in CH_2Cl_2 and of electrochemically generated $12^{\bullet-}$ (bottom) in $\text{CH}_2\text{Cl}_2/0.1 \text{ M Bu}_4\text{NPF}_6$ at 295 K.

EPR signal with $g = 2.002$ and detectable hyperfine coupling to the ^{14}N and ^{105}Pd nuclei (Table 4).^{11f} We were also able to

Table 4. EPR Parameters of the Complexes from Measurements in X-band^a

compd	g_{iso}	
$1^{\bullet-}$	1.986	
$12^{\bullet-}$	2.003	
$2^{\bullet-}$	1.988	$2a(^{195}\text{Pt}) = 50 \text{ G}^{b,c}$
$3^{\bullet-}$	2.002	$a(^{14}\text{N}) = 4.5, 6 \text{ G}; a(^{105}\text{Pd}) = 5 \text{ G}^{d-f}$

^aX-band EPR data obtained from *in situ* generated species in $\text{CH}_2\text{Cl}_2/0.1 \text{ M Bu}_4\text{NPF}_6$ at 298 K. ^bIsotropic hyperfine coupling constants in gauss obtained from simulation. ^cHyperfine coupling to ^{195}Pt , $I = 1/2$, natural abundance 33.3%. ^dHyperfine coupling to ^{105}Pd , $I = 5/2$, natural abundance 22.2%. ^eHyperfine coupling to ^{14}N , $I = 1$. ^fFrom ref 11f.

record the EPR spectrum of the two-electron-reduced species $12^{\bullet-}$. The latter displays a line-rich EPR spectrum at 295 K in $\text{CH}_2\text{Cl}_2/0.1 \text{ M Bu}_4\text{NPF}_6$ centered at $g = 2.003$ (Figure 5). The poor signal-to-noise ratio, coupled with the complex nature of the signal, precluded a reasonable simulation of this spectrum. For $12^{\bullet-}$, which contains two spins, either the singlet or the triplet state could be the ground state of this molecule. The detection of an EPR signal at 295 K proves that the triplet state is populated at 295 K. Molecule **1** contains two redox-active ligands, az_H and Q_H. Since the EPR spectrum of $1^{\bullet-}$ does not contain any hyperfine structure, we turned to DFT calculations to further investigate the electronic structures of that redox form.

Structure-based DFT calculations were carried out for the various redox forms of **1**. Structural optimization of **1** with the BP-86 functional reproduced the bond lengths and bond angles with reasonable accuracy (Tables S2 and S3, Supporting Information). A look at the spin densities calculated according to the Löwdin population analysis for $1^{\bullet-}$ shows that the spin

density is equally distributed between the Q_{H} and az_{H} ligands (Figure 6). Thus, taken together, the EPR and DFT

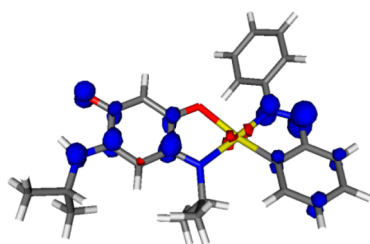


Figure 6. DFT calculated spin density plot of $1^{\bullet-}$.

calculations suggest that the $1^{\bullet-}$ form is best described as a combination of $[(az_{\text{H}})Pt^{II}(Q_{\text{H}})]^{\bullet-}$ and $[(az_{\text{H}})^{\bullet-}Pt^{II}(Q_{\text{H}})]^{\bullet-}$. Interestingly, the corresponding Pd(II) complex $3^{\bullet-}$ was formulated by us as $[(az_{\text{H}})^{\bullet-}Pd^{II}(Q_{\text{H}})]^{\bullet-}$ on the basis of hyperfine information from EPR spectroscopy.^{11f} Calculation of spin density for $3^{\bullet-}$ shows about 80% spin density on the az_{H} part and supports the $[(az_{\text{H}})^{\bullet-}Pd^{II}(Q_{\text{H}})]^{\bullet-}$ formulation (Figure S2, Supporting Information). Hence, on changing the metal center from Pd(II) in $3^{\bullet-}$ to Pt(II) in $1^{\bullet-}$, the locus of the first electron transfer changes from a predominantly az_{H} -localized to a ligand-delocalized situation. For 1^{2-} , we were not able to generate reasonable calculated data. This problem is likely associated with the high negative charge of 1^{2-} , which makes calculations on such systems inaccurate.

The one-electron-reduced form $2^{\bullet-}$ of the dinuclear complex displays an EPR signal in CH_2Cl_2 at 295 K centered at $g = 1.988$ (Figure 7). This signal could be simulated by considering

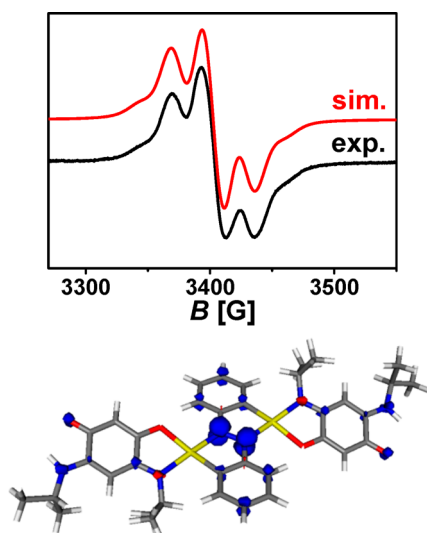


Figure 7. X-band EPR spectrum of $2^{\bullet-}$ in CH_2Cl_2 at 295 K together with a simulation (top). DFT calculated spin density plot of $2^{\bullet-}$ (bottom).

a hyperfine coupling to two ^{195}Pt ($I = 1/2$, natural abundance 33.3%) nuclei of 50 G. The two-electron-reduced form 2^{2-} turned out to be EPR silent. Structure-based DFT calculations were also carried out on the various redox forms of **2**. Optimization of the structure of **2** was carried out with the BP86 functional, and the calculated bond lengths and bond angles show a reasonable match with the experimental values

(Tables S2 and S3, Supporting Information). A look at the spin density calculated according to the Löwdin population analysis shows about 70% spin density on the $az_{2\text{H}}$ part in $2^{\bullet-}$. Hence $2^{\bullet-}$ can be best formulated as $[(Q_{\text{H}})Pt^{II}(\mu\text{-}az_{2\text{H}})^{\bullet-}Pt^{II}(Q_{\text{H}})]^{\bullet-}$ (Figure 7).

For the two-electron-reduced form 2^{2-} , DFT calculations delivered a broken-symmetry solution with an energy difference between the triplet and the singlet state of 1168 cm^{-1} , thus clearly establishing the singlet state as the ground state for that molecule. Taking together the DFT-supported stabilization of the singlet ground state, the EPR silence of 2^{2-} , and the known tendency of azo-based ligands to undergo facile reduction upon double metalation, 2^{2-} is best formulated as $[(Q_{\text{H}})Pt^{II}(\mu\text{-}az_{2\text{H}})^{2-}Pt^{II}(Q_{\text{H}})]^{2-}$. The two-electron reduction thus results in a hydrazido type of bridge. The EPR results and spin-density calculations thus show that the locus of reduction in such complexes can be shifted from a delocalized situation to a localized one by changing the metal center ($1^{\bullet-}$ vs $3^{\bullet-}$) or on going from a mononuclear to a dinuclear complex ($1^{\bullet-}$ vs $2^{\bullet-}$).

UV–Vis–Near-IR Spectroelectrochemistry and TD-DFT Calculations. Complex **1** exhibits several absorption bands in the visible and ultraviolet region. The main bands in the visible and UV regions are observed at 527, 486, 446, 387, and 354 nm, all of which are intense (Figure 8 and Table 5). TD-DFT

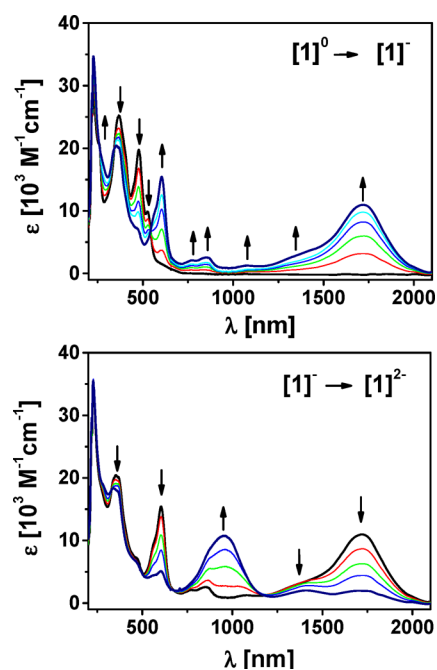


Figure 8. Changes in the UV–vis–near-IR spectrum of **1** during the reduction steps from OTTLE spectroelectrochemistry in $\text{CH}_2\text{Cl}_2/0.1\text{ M Bu}_4\text{NPF}_6$.

calculations on **1** help in the assignment of these bands. The relevant frontier orbitals are shown in Figure 9, and the data are summarized in Table 6. All of these bands possess a mixed ligand to ligand charge-transfer (LLCT) and/or metal to ligand charge-transfer (MLCT) character. This description fits with the intuitive idea of the Q_{H} - and Pt-based orbitals predominantly contributing to the filled orbitals and the Q_{H} - and az_{H} -based orbitals contributing to the empty receptor orbitals in **1**. Additional bands in the UV region are assigned to a $\pi\text{-}\pi^*$ ligand-centered transition. The absorption bands for the corresponding mononuclear Pd(II) complex are much

Table 5. UV–vis–Near-IR Absorption Data of the Complexes in the Various Redox States^a

	λ (nm) (ϵ (10^3 M ⁻¹ cm ⁻¹))
1 ⁰	234 (23.4); 261 (19.8); 354 (19.2); 387 (19.2); 446 sh; 486 (18.9); 527 (10.1); 617 sh
1 ^{•-}	227 (34.6); 270 sh; 352 (20.4); 466 sh; 562 sh; 604 (15.4); 768 (2.1); 854 (2.6); 1068 sh; 1427 sh; 1720 (11.0)
1 ²⁻	227 (35.5); 280 sh; 339 (18.4); 366 sh; 469 sh; 559 sh; 604 (5.1); 854 (10.8); 1074 sh; 1416 (2.0); 1729 (2.0)
2 ⁰	234 (44.4); 273 sh; 340 (23.8); 404 (33.6); 550 (29.0); 612 (41.7); 913 (3.2)
2 ^{•-}	228 (74.9); 367 (44.6); 412 sh; 567 sh; 612 (32.9); 1350 (9.0)
2 ²⁻	229 (75.5); 305 (33.1); 361 (41.6); 615 (15.5); 953 (7.3); 1302 sh; 1775 (26.0)
2 ³⁻	229 (77.2); 311 (38.1); 339 (37.9); 444 sh; 582 (11.1); 954 (16.8); 1072 (13.8); 1321 sh; 1768 (16.9)
3 ^{0 b}	359 (20.50); 407 (17.50); 485 sh; 560 (0.82)
3 ^{•- b}	360 sh; 397 (19.70); 557 (3.50); 650 sh; 1415 (1.650)
3 ^{2- b}	329 (14.70); 386 (12.50); 490 (4.80); 605 sh; 908 (3.40)

^aFrom OTTLE spectroelectrochemistry in CH₂Cl₂/0.1 M Bu₄NPF₆ at 295 K. ^bFrom ref 11f.

weaker in intensity (Table 5). Hence, replacing Pd(II) in **3** by Pt(II) in **1** results in an improvement of the oscillator strengths of the transitions, possibly due to better orbital overlap in **3**.^{11f} Introduction of a second “Pt(Q_H)” unit on going to **2** leads to a doubling of intensity of all the absorption bands (Figure S3 (Supporting Information), Figure 10, and Table 5). Additionally, all absorption bands (except those appearing in the UV region) exhibit a bathochromic shift on going from the mononuclear complex **1** to the dinuclear complex **2**; the main bands in the UV–vis region for **2** appear at 612, 550, 404, and 340 nm. Additionally, there is a weak band at 913 nm in the near-IR region. The band patterns are similar for both complexes. Relevant calculated frontier orbitals for the transitions observed in **2** are displayed in Figure 11. The LUMO and LUMO+1 orbitals of **2** are localized on the az_{2H} and Q_H orbitals, respectively. TD-DFT supports the assignment of the band at 612 nm as a predominantly dπ(Pt) to π*(az_{2H}) MLCT transition (Figure 11 and Table 6). The band at 550 nm has a mixed MLCT/LLCT character, and that at 404 nm has a predominantly dπ(Pt) to π*(Q_{2H}) MLCT character.

The one-electron reduction of **1** leads to a slight decrease in the intensity of the band at 354 nm. The bands at 486 and 527 nm disappear on one-electron reduction, and a new band appears at 604 nm (Figure 8 and Table 5). This band is assigned to a mixed MLCT/LLCT transition. Whereas **1** is

transparent in the near-IR region, its reduction to **1**^{•-} leads to the appearance of a strong absorption band at 1720 nm. This near-IR band is assigned to a π to π* transition from within the resonance-stabilized forms [(az_H)Pt^{II}(Q_H)^{•-}]^{•-} and [(az_H)^{•-}Pt^{II}(Q_H)]^{•-} (see EPR Spectroscopy and Spin-Density Calculations). Further reduction to **1**²⁻ leads to a drastic loss in intensity in all the vis–near-IR bands of **1**^{•-}, except for that at 339 nm (Figure 8). Furthermore, for **1**²⁻ a new intense band appears at 854 nm. This band is tentatively assigned to a metal-to-ligand-charge-transfer (MLCT) transition within the complex [(az_H)^{•-}Pt^{II}(Q_H)^{•-}]²⁻.

The reduction of the dinuclear complex **2** to **2**^{•-} leads to a loss in intensity of all the bands in the visible region (Figure 9). Additionally, a broad band centered at 1350 nm appears in the near-IR region. This band is assigned to a (az_{2H})^{•-} to (Q_H) LLCT transition within the formulation [(Q_H)Pt^{II}(μ-az_{2H})^{•-}Pt^{II}(Q_H)]^{•-}. Reduction of **2**^{•-} to **2**²⁻ leads to an increase in intensity of the near-IR band, and its bathochromic shift to 1775 nm. This band is also LLCT in character. The bathochromic shift and the increase in intensity of this band can be explained by considering the formulation [(Q_H)Pt^{II}(μ-az_{2H})²⁻Pt^{II}(Q_H)]²⁻, with the transition taking place from (az_{2H})²⁻ to (Q_H). The presence of an additional electron on az_{2H} on going from **2**^{•-} to **2**²⁻ (see EPR Spectroscopy and Spin-Density Calculations) would account for the bathochromic shift and the increase in intensity of the LLCT band. All bands in the visible region lose intensity on reducing **2**^{•-} to **2**²⁻. Reduction of **2**²⁻ to **2**³⁻ leads to a decrease in the intensity of the LLCT band, as would be expected for a formulation [(Q_H)^{•-}Pt^{II}(μ-az_{2H})²⁻Pt^{II}(Q_H)]³⁻, which contains one hole less on Q_H than in **2**²⁻. Two new bands appear for **2**³⁻ at 954 and 1072 nm, and these are tentatively assigned to MLCT transitions.

CONCLUSIONS

Summarizing, we have presented here the mononuclear Pt(II) complex **1** and the dinuclear Pt(II) complex **2**, which contain different redox-active ligands. **2** is a rare example of a metal complex where the ligand az acts as a bridging ligand in its doubly deprotonated form. Structural characterization of the complexes shows bond localization within the Q_H ligand in comparison to free Q. A combination of electrochemical, EPR spectroelectrochemical, and DFT studies was used to unravel the electronic structures of these complexes in the various redox states (together with the Pd(II) analogue **3**), and the results can be summarized as shown in Scheme 2.

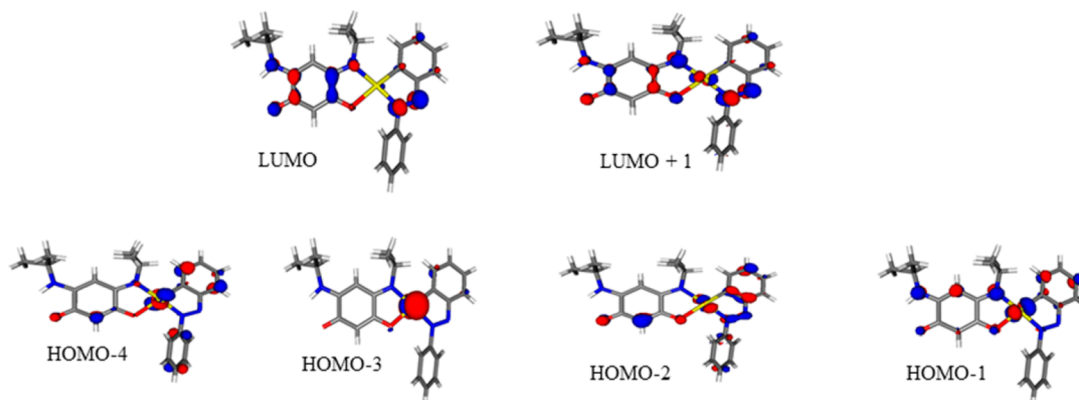


Figure 9. Relevant calculated frontier orbitals (canonical orbitals) for the optical transitions observed in **1** (see Table 6 for details).

Table 6. Main TD-DFT Calculated Transitions of **1** and **2** in Comparison with Experimental Data

compd	main contributing excitation (%)	transition maximum (nm)	oscillator strength	exptl transition maximum (nm) ^a	molar abs coefficient (M ⁻¹ cm ⁻¹), ^a band assignment
1	HOMO-1 → LUMO (57)	502	0.172	527	10100, M/L → L
	HOMO-2 → LUMO (22)				
	HOMO-2 → LUMO (46)	473	0.163	486	18900, M/L → L
	HOMO-1 → LUMO (25)				
	HOMO-2 → LUMO (34)	438	0.218	446	sh, M → L
	HOMO-3 → LUMO (31)				
	HOMO-4 → LUMO (35)	398	0.106	387	19200, M/L → L
	HOMO-1 → LUMO+1 (25)				
2	HOMO-4 → LUMO+1 (40)	325	0.135	354	19200, M/L → L
	HOMO-2 → LUMO (80)	599	0.678	612	41700, M → L
	HOMO-4 → LUMO (72)	520	0.349	550	29000, M/L → L
	HOMO-3 → LUMO+1 (53)	420	0.187	404	33600, M → L
	mixed	331	0.228	340	23800

^aData from OTTLE spectroelectrochemistry in CH₂Cl₂/0.1 M Bu₄NPF₆.

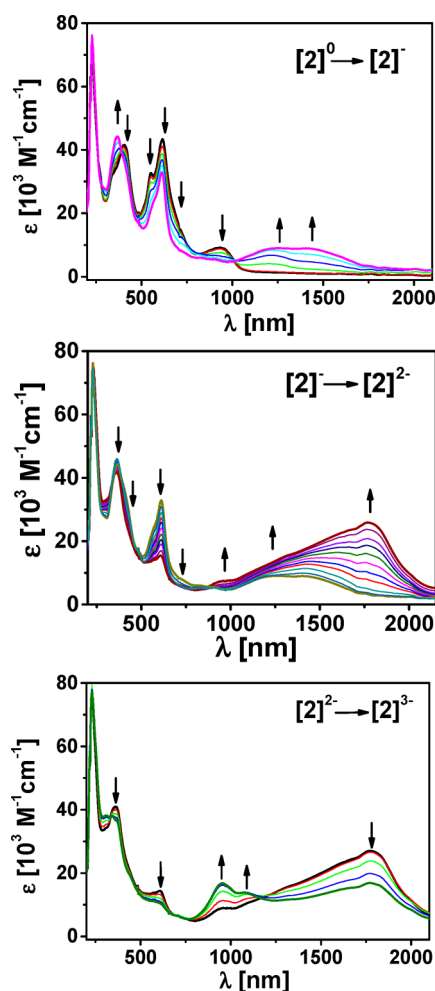


Figure 10. Changes in the UV-vis-near-IR spectrum of **2** during the reduction steps from OTTLE spectroelectrochemistry in CH₂Cl₂/0.1 M Bu₄NPF₆.

The locus of reduction can thus be shifted by changing either the metal center (**1** vs **3**) or the nuclearity of the metal complexes (**1** vs **2**). Furthermore, the complexes have been shown to absorb light in either the visible or the near-IR region depending on their redox states. Thus, the position and intensity of light absorption in these complexes can be tuned by

simple electron-transfer steps. Absorption in the visible as well as the near-IR regions can be switched on and off by performing redox processes in the complexes, making them highly electrochromic.¹⁵ It is the combination of different redox-active chromophores that makes this electrochromic behavior possible. We note that all electron transfer processes that lead to the electrochromic behavior in these complexes are ligand based.

EXPERIMENTAL SECTION

General Considerations. The ligand Q^{11d} and the complex [(az_H)Pt(μ-Cl)₂Pt(az_H)]² were prepared according to reported procedures. All other reagents are commercially available and were used as received. All solvents were dried and distilled using common techniques unless otherwise mentioned.

Instrumentation. ¹H and ¹³C NMR spectra were recorded at JEOL LAMBDA 400 (400 MHz) instrument. Cyclic voltammetry was carried out in 0.1 M Bu₄NPF₆ solution using a three-electrode configuration (glassy-carbon working electrode, Pt counter electrode, Ag wire as pseudoreference) and PAR 273 potentiostat and function generator. The ferrocene/ferrocenium (Fc/Fc⁺) couple served as internal reference. The EPR spectroelectrochemistry for 1^{•-} and 1²⁻ was carried out in a cell using a laminated Pt-mesh working electrode, a Pt-wire counter electrode, and a silver-wire quasi-reference electrode. The cell was filled with a solution in a glovebox and then tightly closed and transferred into the cavity of an X-band EPR spectrometer (EMX Bruker, Germany), where the spectroelectrochemical measurements were done. Potentials were controlled by a HEKA potentiostat/galvanostat system (HEKA Elektronik, Lambrecht/Pfalz, Germany). Chemical generation of paramagnetic 2^{•-} was carried out by reaction of the substance with cobaltocene under an argon atmosphere. EPR spectra were recorded with a Bruker System EMX instrument. Simulations of EPR spectra were done using the EasySpin program.¹⁶ UV-vis-near-IR absorption spectra were recorded on an Avantes spectrometer system: Ava Light-DH-BAL (light source), AvaSpec-ULS2048 (UV-vis detector), and AvaSpec-NIR256-2.5TEC (near-IR-detector). Spectroelectrochemical measurements were carried out using an optically transparent thin-layer electrochemical (OTTLE) cell.¹⁷ Elemental analysis was performed on an ELEMENTAR Vario EL III instrument. Mass spectrometry experiments were carried out on an Agilent 6210 ESI-TOF mass spectrometer (Agilent Technologies, Santa Clara, CA).

Synthesis of Complexes 1 and 2. A mixture of ligand Q (46 mg, 0.2 mmol) and KO-*t*-Bu (24 mg, 0.2 mmol) in tetrahydrofuran (15 mL) was stirred for 8 h at room temperature. The suspension changed from deep red to yellow-orange. The solvent was removed in vacuo. The complex [Pt(az_H)(μ-Cl)₂] (82 mg, 0.1 mmol) and dichloromethane (15 mL) were added to the yellow precipitate. The reaction

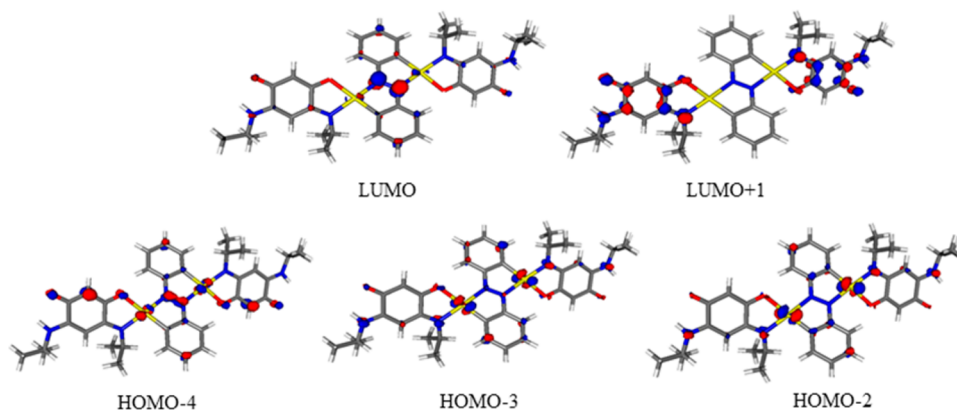
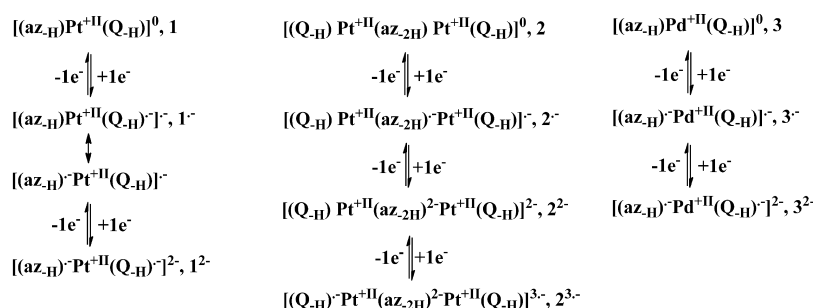


Figure 11. Relevant calculated frontier orbitals (canonical orbitals) for the optical transitions observed in **2** (see Table 6 for details).

Scheme 2. Redox Scheme



mixture was stirred for 24 h at room temperature. The solution turned black. The solution was filtered, and the solvent was evaporated. The black residue was extracted with 10 mL of *n*-heptane, the suspension was filtered, and the filtrate was concentrated. The deep red complex **1** was recrystallized from dichloromethane/*n*-hexane (2 mL/10 mL). The precipitate was filtered, washed with *n*-hexane, and dried in vacuo. Yield: 44.4 mg (0.069 mmol, 34.5%). ^1H NMR (400 MHz, CDCl_3): δ 1.29 (d, 6H, $J = 6.5$ Hz, *i*-Pr); 1.66 (d, 6H, $J = 7.1$ Hz, *i*-Pr); 3.65 (multiplet, 1H, $J = 6.6$ Hz, *i*-Pr); 4.90 (sept, 1H, $J = 7.1$ Hz, *i*-Pr); 5.42 (s, 1H, quinone); 5.47 (s, 1H, quinone); 6.58 (d, 1H, $J = 7.8$ Hz, NH); 7.24 (m, 1H, azobenzene); 7.35 (m, 1H, azobenzene); 7.49 (m, 4H, azobenzene); 7.91 (m, 2H, azobenzene); 8.07 (dd, 1H, $J = 7.7$ Hz, $J = 1.4$ Hz, azobenzene). $^{13}\text{C}\{^1\text{H}\}$ NMR (100 MHz, CDCl_3): δ 21.67; 21.97; 31.01; 44.39; 57.33; 87.60; 103.41; 124.34; 124.94; 128.35; 129.56; 130.97; 132.31; 132.75; 140.47; 145.83; 151.67; 165.53; 170.92; 178.94; 182.21. Anal. Calcd for $\text{C}_{24}\text{H}_{26}\text{N}_4\text{O}_2\text{Pt} \cdot 0.5\text{CH}_2\text{Cl}_2$: C, 45.98; H, 4.25; N, 8.75. Found: C, 45.86; H, 4.24; N, 8.68. HRMS (ESI): calcd for $\text{C}_{24}\text{H}_{27}\text{N}_4\text{O}_2\text{Pt}$ ($[\text{M} + \text{H}]^+$), m/z 598.1778; found, m/z 598.1798.

After the extraction with *n*-heptane, the blue residue was recrystallized from chloroform/*n*-hexane (5 mL/15 mL). The blue compound **2** was filtered, washed with *n*-hexane, and dried in vacuo. Yield: 24.3 mg (0.024 mmol, 24%). ^1H NMR (400 MHz, CDCl_3): δ 1.32 (d, 6H, $J = 6.4$ Hz, *i*-Pr); 1.66 (d, 6H, $J = 7.1$ Hz, *i*-Pr); 3.67 (multiplet, 1H, $J = 6.6$ Hz, *i*-Pr); 5.02 (sept, 1H, $J = 7.1$ Hz, *i*-Pr); 5.50 (s, 1H, quinone); 5.65 (s, 1H, quinone); 6.64 (d, 1H, $J = 8.1$ Hz, NH); 7.27 (m, 2H, azobenzene); 7.49 (m, 1H, $J = 7.7$ Hz, azobenzene); 9.14 (m, 1H, azobenzene). $^{13}\text{C}\{^1\text{H}\}$ NMR (100 MHz, CDCl_3): δ 14.19; 21.90; 21.98; 22.73; 31.66; 44.49; 53.49; 57.95; 88.20; 103.43; 125.37; 126.75; 131.75; 145.85; 178.99; 182.22. Anal. Calcd for $\text{C}_{36}\text{H}_{42}\text{N}_6\text{O}_4\text{Pt}_2$: C, 42.69; H, 4.18; N, 8.30. Found: C, 42.76; H, 4.41; N, 8.30. HRMS (ESI): calcd for $\text{C}_{36}\text{H}_{43}\text{N}_6\text{O}_4\text{Pt}_2$ ($[\text{M} + \text{H}]^+$), m/z 1013.2630; found, m/z 1013.2625.

X-ray Crystallography. Single crystals of **1** were obtained by layering a dichloromethane solution of **1** with *n*-hexane (1/5) and allowing for slow diffusion at ambient temperature. Single crystals of **2** were grown by slow diffusion of diethyl ether into an acetone solution

of **2**. Intensity data were collected at 100(2) K on a BRUKER Smart AXS diffractometer (graphite-monochromated Mo $K\alpha$ radiation, $\lambda = 0.71073$ Å). Crystallographic and experimental details for the structures are summarized in Table S1 (Supporting Information). Structures were solved by direct methods (SHELXS-97) and refined by full-matrix least-squares procedures (based on F^2 , SHELXL-97).¹⁸ CCDC 933111 and 933110 contain CIF files for this paper. All data can be obtained free of charge from the Cambridge Crystallographic Data Centre via www.ccdc.cam.ac.uk/data_requests/cif.

DFT Calculations. DFT calculations were performed with the ORCA 2.9.1 program package¹⁹ using the BP86 and B3LYP functionals for the geometry optimization and single-point calculations, respectively.²⁰ Empirical van der Waals corrections were utilized for the geometry optimization.²¹ Default convergence criteria were set for the geometry optimization (OPT) and tight convergence criteria for SCF calculations (TIGHTSCF). Relativistic effects were included with the zeroth-order relativistic approximation (ZORA).²² Triple- ζ valence basis sets with polarization functions (TZVPP-ZORA)²³ were employed for all atoms. The resolution of the identity approximation²⁴ was used with matching auxiliary basis sets. Time-dependent DFT (TD-DFT) was employed to calculate the low-lying excitation energies. Solvent effects were taken into account with the conductor-like screening model (COSMO)²⁵ for all calculations. Spin densities were calculated according to the Löwdin population analysis.²⁶ Molecular orbitals and spin densities were visualized with the Molekel program.²⁷

■ ASSOCIATED CONTENT

📄 Supporting Information

CIF files and tables giving the crystallographic details for **1** and **2**, figures giving ^1H NMR spectra of **1** and **2**, a spin density plot of $\mathbf{3}^{2-}$, and UV-vis-near-IR spectra of **1** and **2**, and tables showing a comparison of calculated and experimental bond lengths and bond angles for **1** and **2** and coordinates of DFT calculations. This material is available free of charge via the Internet at <http://pubs.acs.org>.

AUTHOR INFORMATION

Corresponding Author

*E-mail for B.S.: Biprajit.sarkar@fu-berlin.de.

Notes

The authors declare no competing financial interest.

ACKNOWLEDGMENTS

We are indebted to the Carl-Zeiss Stiftung (doctoral stipend for N.D.) and the Fonds der Chemischen Industrie (Chemiefondsstipendium for M.G.S.) for financial support of this project. The ZEDAT, FU Berlin, is acknowledged for access to the computing center. We are grateful to Prof. Dr. L. Dunsch for access to the instrumental facilities of IFW Dresden for the EPR measurements of $1^{•-}$ and 1^{2-} .

REFERENCES

- (1) (a) Bandara, H. M. D.; Burdette, S. C. *Chem. Soc. Rev.* **2012**, *41*, 1809 and references therein. (b) Kirsch, H.; Holzmeier, P. *Adv. Organomet. Chem.* **1992**, *34*, 67. (c) Yukuta, T.; Mori, L.; Kurihara, M.; Mizutani, J.; Tamai, N.; Kawai, T.; Irie, M.; Nishihara, H. *Inorg. Chem.* **2002**, *41*, 7143. (d) Kume, S.; Nishihara, H. *Dalton Trans.* **2008**, 3260. (e) Hirade, T.; Okui, Y.; Han, M. N. *J. Mater. Chem. C* **2013**, *1*, 2672.
- (2) Cope, A. C.; Siekman, R. W. *J. Am. Chem. Soc.* **1965**, *87*, 3272.
- (3) For selected examples see: (a) Sarkar, B.; Patra, S.; Fiedler, J.; Sunoj, R. B.; Janardanan, D.; Lahiri, G. K.; Kaim, W. *J. Am. Chem. Soc.* **2008**, *130*, 3532. (b) Santra, B.; Thakur, G. A.; Ghosh, P.; Pramanik, A.; Lahiri, G. K. *Inorg. Chem.* **1996**, *35*, 3050. (c) Lahiri, G. K.; Bhattacharya, S.; Goswami, S.; Chakravorty, A. *J. Chem. Soc., Dalton Trans.* **1990**, 561. (d) Sarkar, B.; Huebner, R.; Pattacini, R.; Hartenbach, I. *Dalton Trans.* **2009**, 4653. (e) Deibel, N.; Schweinfurth, D.; Fiedler, J.; Zalis, S.; Sarkar, B. *Dalton Trans.* **2011**, *40*, 9925. (f) Deibel, N.; Schweinfurth, D.; Hohloch, S.; Sarkar, B. *Inorg. Chim. Acta* **2012**, *380*, 269. (g) Deibel, N.; Schweinfurth, D.; Hohloch, S.; Fiedler, J.; Sarkar, B. *Chem. Commun.* **2012**, *48*, 2388. (h) Paul, N. D.; Rana, U.; Goswami, S.; Mondal, T. K.; Goswami, S. *J. Am. Chem. Soc.* **2012**, *134*, 6520. (i) Das, A.; Scherer, T. M.; Mobin, S. M.; Kaim, W.; Lahiri, G. K. *Chem. Eur. J.* **2012**, *18*, 11007. (j) Sarkar, B.; Patra, S.; Fiedler, J.; Sunoj, R. B.; Janardanan, D.; Mobin, S. M.; Niemeyer, M.; Lahiri, G. K.; Kaim, W. *Angew. Chem., Int. Ed.* **2005**, *44*, 5655. (k) Baldwin, D. A.; Lever, A. B. P.; Parish, R. V. *Inorg. Chem.* **1969**, *8*, 107.
- (4) (a) Kaim, W. *Coord. Chem. Rev.* **2001**, 219–221, 463. (b) Samanta, S.; Ghosh, P.; Goswami, S. *Dalton Trans.* **2012**, *41*, 2213.
- (5) For selected examples see (a) Babic, D.; Curic, M.; Molcanov, K.; Ilc, G.; Plavec, J. *Inorg. Chem.* **2008**, *47*, 10446. (b) Roy, S.; Hartenbach, I.; Sarkar, B. *Eur. J. Inorg. Chem.* **2009**, 2553. (c) Moustafa, M. E.; McCreedy, M. S.; Puddphatt, R. J. *Organometallics* **2012**, *31*, 6262. (d) Juribasic, M.; Curic, M.; Molcanov, K.; Matkovic-Calogovic, D.; Babic, D. *Dalton Trans.* **2010**, 39, 8769. (e) Han, M.; Hirade, T.; Hara, M. *New J. Chem.* **2010**, *34*, 2887.
- (6) (a) Yamamoto, Y.; Yamazaki, H. *J. Org. Chem.* **1977**, *42*, 4136. (b) Bennett, R. L.; Bruce, M. I.; Goodall, B. L.; Stone, F. G. A. *Aust. J. Chem.* **1974**, *27*, 2131. (c) Siedle, A. R. *J. Organomet. Chem.* **1981**, *208*, 115. (d) Bruce, M. I.; Liddell, M. J.; Snow, M. R.; Tiekink, E. R. T. *Aust. J. Chem.* **1988**, *41*, 1407. (e) Evans, W. J.; Drummond, D. K.; Chamberlain, L. R.; Doedens, R. J.; Bott, S. G.; Zhang, H.; Atwood, J. L. *J. Am. Chem. Soc.* **1988**, *110*, 4983. (f) Zhambrano, C. H.; Sharp, P. R.; Barnes, C. L. *Organometallics* **1995**, *14*, 3607. (g) Curic, M.; Babic, D.; Visnjevac, A.; Molcanov, K. *Inorg. Chem.* **2005**, *44*, 5975. (h) Hoover, J. M.; Freudenthal, J.; Michael, F. E.; Mayer, J. M. *Organometallics* **2008**, *27*, 2238. (i) Cincic, D.; Juribasic, M.; Babic, D.; Molcanov, K.; Sket, P.; Plavec, J.; Curic, M. *Chem. Commun.* **2011**, *47*, 11543.
- (7) (a) Braunstein, P.; Siri, O.; Taquet, J.-P.; Rohmer, M.-M.; Bénard, M.; Walter, R. *J. Am. Chem. Soc.* **2003**, *125*, 12246. (b) Yang, Q.-Z.; Siri, O.; Braunstein, P. *Chem. Commun.* **2005**, 2660. (c) Yang, Q.-Z.; Siri, O.; Braunstein, P. *Chem. Eur. J.* **2005**, *11*, 7237.
- (8) (a) Kunkel, D. A.; Simpson, S.; Nitz, J.; Rojas, G. A.; Zurek, E.; Routaboul, L.; Doudin, B.; Braunstein, P.; Dowben, P. A.; Enders, A. *Chem. Commun.* **2012**, *48*, 7143. (b) Routaboul, L.; Braunstein, P.; Xiao, J.; Zhang, Z.; Dowben, P. A.; Dalmás, G.; da Costa, V.; Felix, O.; Decher, G.; Rosa, L. G.; Doudin, B. *J. Am. Chem. Soc.* **2012**, *134*, 8494. (c) Rosa, L. G.; Velev, J.; Zhang, Z.; Alvira, J.; Vega, O.; Diaz, G.; Routaboul, L.; Braunstein, P.; Doudin, B.; Losovjy, Y. B.; Dowben, P. A. *Phys. Status Solidi B* **2012**, *249*, 1571. (d) Dowben, P. A.; Kunkel, D. A.; Enders, A.; Rosa, L. G.; Routaboul, L.; Doudin, B.; Braunstein, P. *Top. Catal.* **2013**, *56*, 1096.
- (9) (a) Kauf, T.; Braunstein, P. *Dalton Trans.* **2011**, *40*, 9967. (b) Kauf, T.; Braunstein, P. *Inorg. Chem.* **2011**, *50*, 11472.
- (10) (a) Yang, Q.-Z.; Kermagoret, A.; Agostinho, M.; Siri, O.; Braunstein, P. *Organometallics* **2006**, *25*, 5518. (b) Hohloch, S.; Braunstein, P.; Sarkar, B. *Eur. J. Inorg. Chem.* **2012**, 546.
- (11) (a) Siri, O.; Taquet, J.-P.; Collin, J.-P.; Rohmer, M.-M.; Bénard, M.; Braunstein, P. *Chem. Eur. J.* **2005**, *11*, 7247. (b) Cotton, F. A.; Jin, J.-Y.; Li, Z.; Murillo, C. A.; Reibenspies, J. H. *Chem. Commun.* **2008**, 211. (c) Das, H. S.; Das, A. K.; Pattacini, R.; Huebner, R.; Sarkar, B.; Braunstein, P. *Chem. Commun.* **2009**, 4387. (d) Braunstein, P.; Bubrin, D.; Sarkar, B. *Inorg. Chem.* **2009**, *48*, 2534. (e) Paretzki, A.; Pattacini, R.; Huebner, R.; Braunstein, P.; Sarkar, B. *Chem. Commun.* **2010**, *46*, 1497. (f) Deibel, N.; Schweinfurth, D.; Huebner, R.; Braunstein, P.; Sarkar, B. *Dalton Trans.* **2011**, *40*, 431.
- (12) (a) Das, H. S.; Weisser, F.; Schweinfurth, D.; Su, C.-Y.; Bogani, L.; Fiedler, J.; Sarkar, B. *Chem. Eur. J.* **2010**, *16*, 2977. (b) Schweinfurth, D.; Das, H. S.; Weisser, F.; Bubrin, D.; Sarkar, B. *Inorg. Chem.* **2011**, *50*, 1150. (c) Weisser, F.; Huebner, R.; Schweinfurth, D.; Sarkar, B. *Chem. Eur. J.* **2011**, *17*, 5727. (d) Sommer, M. G.; Schweinfurth, D.; Weisser, F.; Hohloch, S.; Sarkar, B. *Organometallics* **2013**, *32*, 2069. (e) Schweinfurth, D.; Khusniyarov, M. M.; Bubrin, D.; Hohloch, S.; Su, C.-Y.; Sarkar, B. *Inorg. Chem.* **2013**, *52*, 10332.
- (13) (a) Kumbhakar, D.; Sarkar, B.; Maji, S.; Mobin, S.; Fiedler, J.; Aparicio, R. J.; Kaim, W.; Lahiri, G. K. *J. Am. Chem. Soc.* **2008**, *130*, 17575. (b) Keyer, T. E.; Forster, R. J.; Jayaweera, P. M.; Coates, C. G.; McGarvey, J. J.; Vos, J. G. *Inorg. Chem.* **1998**, *37*, 5925. (c) Kar, S.; Sarkar, B.; Ghuman, S.; Janardanan, D.; van Slageren, J.; Fiedler, J.; Puranik, V. G.; Sunoj, R. B.; Kaim, W.; Lahiri, G. K. *Chem. Eur. J.* **2005**, *11*, 4901. (d) Zhang, D.; Jin, G.-X. *Organometallics* **2003**, *22*, 2851. (e) Scheuermann, S.; Kretz, T.; Vitze, H.; Bats, J. W.; Bolte, M.; Lerner, H. W.; Wagner, M. *Chem. Eur. J.* **2008**, *14*, 2590. (f) Mattsson, J.; Govindaswamy, P.; Renfrew, A. K.; Dyson, P. J.; Stepnicka, P.; Süß-Fink, G.; Therrien, B. *Organometallics* **2009**, *28*, 4350. (g) Margraf, G.; Kretz, T.; de Biani, F. F.; Lasi, F.; Loschi, S.; Zanello, P.; Bats, J. W.; Wolf, J.; Removic-Langer, K.; Lang, M.; Prokofiev, A.; Assmus, W.; Lerner, H.-W.; Wagner, M. *Inorg. Chem.* **2006**, *45*, 1277.
- (14) Patra, S.; Sarkar, B.; Mobin, S. M.; Kaim, W.; Lahiri, G. K. *Inorg. Chem.* **2003**, *42*, 6469.
- (15) (a) Kaim, W. *Coord. Chem. Rev.* **2011**, 255, 2503. (b) Chen, J.; Winter, R. F. *Chem. Eur. J.* **2012**, *18*, 10733. (c) Ward, M. D. *J. Solid State Electrochem.* **2005**, *9*, 778. (d) Mortimer, R. J. *Comprehensive Coord. Chem.* **2004**, *9*, 581.
- (16) Stoll, S.; Schweiger, A. *J. Magn. Reson.* **2006**, *178*, 42.
- (17) Krejčík, M.; Danek, M.; Hartl, F. J. *Electroanal. Chem.* **1991**, *317*, 179.
- (18) Sheldrick, G. M. *SHELXL-97, Program for refinement of crystal structures*; University of Göttingen, Göttingen, Germany, 1997.
- (19) Neese, F. *ORCA-an Ab Initio, Density Functional and Semiempirical Program Package, version 2.9.1*; Department of molecular theory and spectroscopy, Max Planck Institute for Bioinorganic Chemistry, Mülheim/Ruhr, Germany, January 2012.
- (20) (a) Becke, A. D. *J. Chem. Phys.* **1993**, *98*, 5648. (b) Becke, A. D. *Phys. Rev. A* **1988**, *38*, 3098. (c) Lee, C.; Yang, W.; Parr, R. G. *Phys. Rev. B* **1988**, *37*, 785.
- (21) Grimme, S.; Antony, J.; Ehrlich, S.; Krieg, H. *J. Chem. Phys.* **2010**, *132*, 154104.
- (22) van Wüllen, C. *J. Chem. Phys.* **1998**, *109*, 392.
- (23) Pantazis, D. A.; Chen, X.-Y.; Landis, C. R.; Neese, F. *J. Chem. Theory Comput.* **2008**, *4*, 908.

- (24) (a) Neese, F. *J. Comput. Chem.* **2003**, *24*, 1740. (b) Neese, F.; Wennmohs, F.; Hansen, A.; Becker, U. *Chem. Phys.* **2009**, *356*, 98. (c) Vahtras, O.; Almlöf, J.; Feyereisen, M. W. *Chem. Phys. Lett.* **1993**, *213*, 514. (d) Whitten, J. L. *J. Chem. Phys.* **1973**, *58*, 4496.
- (25) (a) Klamt, A.; Schüürmann, G. *J. Chem. Soc., Perkin Trans. 2* **1993**, 799. (b) Sinnecker, S.; Rajendran, A.; Klamt, A.; Diedenhofen, M.; Neese, F. *J. Phys. Chem. A* **2006**, *110*, 2235.
- (26) Löwdin, P.-O. *J. Chem. Phys.* **1950**, *18*, 365.
- (27) Portmann, S. *Molekel, version 5.4.0.8*; CSCS/UNI, Geneva, Switzerland, 2009.